# Supergene phases from ferruginous duricrusts: non-destructive microsampling and mineralogy prior to (U-Th)/He geochronological analysis

Karina Patrícia Prazeres Marques[1,2], Thierry Allard[2], Cécile Gautheron[3], Benoît Baptiste[2], Rosella Pinna-Jamme[3], Guillaume Morin[2], Ludovic Delbes[2], Pablo Vidal-Torrado[1]

[1]"Luiz de Queiroz" College of Agriculture, University of São Paulo, 13418-900, Piracicaba, São Paulo, Brazil
[2]Institut de Minéralogie, de Physique des Matériaux et de Cosmochimie, UMR CNRS 7590, Sorbonne Université, F-75252, Paris Cedex 05, France
[3]Université Paris-Saclay, CNRS, GEOPS, 91405, Orsay, France

10   *Correspondence to*: Karina P. Prazeres Marques (karina.marques@usp.br)

**Abstract.** Interpreting the ages of supergene mineralogical phases in laterite is complex because they consist of polycrystalline mixtures of different phases at the microscopic scale that could be crystalized at different epochs. Among the geochronometers, the (U-Th)/He method on hematite and goethite is more used, but ages can be difficult to interpret due to phases mixing. To resolve this issue, this study proposes a methodology for performing detailed mineralogical analysis of

15   hematite and goethite single grains prior to their dating using the (U-Th)/He method. Strictly non-destructive mineralogy of single grains is not achievable by classical tools, such as conventional powder XRD (requiring at least some mg of powder) or SEM (that can contaminate the grain by coating or fixing). Therefore, we have performed X-ray diffraction patterns of single grains using high-flux X-ray beams from both a rotating anode (XRD_rotat) laboratory diffractometer and a synchrotron beamline (XRD_synch) facility, and compared the results in order to design a method based on XRD_rotat only.

20   For this purpose, two samples from the pisolitic facies of a Brazilian ferruginous duricrust (Alto Paranaíba region, Minas Gerais State, Brazil) were chosen because they presented a usual heterogeneity. Rietveld refinements of the XRD patterns obtained from both XRD_rotat and XRD_synch yielded similar results for weight percentage ratio of the main phases, Mean Coherent Domain sizes, and less for Al-substitution rates, thus validating the XRD_rotat approach. No beam-damage was observed when increasing X-ray exposure time, neither on XRD patterns nor (U-Th)/He ages. Hence, inframillimetric,

25   undisturbed grains can be used to analyze the mineralogy of ferruginous duricrusts by XRD_rotat with a short exposure, and the same grains can subsequently be dated by the (U-Th)/He geochronology. The (U-Th)/He dating of pisolitic core and cortex grains also provided meaningful ages: they revealed two evolution phases of the ferruginous duricrust, which occurred at or before the Oligocene for pisolitic core and middle Miocene for pisolitic cortex, agreeing with the previous model for the development of pisoliths. The mineralogy of single grains selected for dating is helpful for discussing the

30   crystallization ages, and the high-flux XRD approach may be applied to other supergene mineral parageneses used for absolute dating of weathering profiles.

# 1 Introduction

Ferruginous duricrusts, containing hematite and/or goethite as major components, consist in hard iron-rich horizons formed at or near the ground surface of laterites that are widespread in intertropical areas (see Tardy, 1993; Tardy and Roquin, 1998).

35   Their modes of formation have been extensively discussed in order to unravel the complexity arising from their polyphasic nature (e.g., McFarlane, 1976; Nahon, 1986; Nahon 1991; Tardy, 1993; Tardy and Roquin, 1998; Ollier and Sheth, 2008). In the landscape, they may represent paleosurfaces that partially resisted erosion and weathering for long periods, down to Mesozoic (e.g., Shuster et al., 2012; Beauvais and Chardon, 2013; Monteiro et al., 2018; Vasconcelos and Carmo, 2018; Vasconcelos et al., 2019). In order to understand and reconstruct related continental surface evolution through time as a

40   result of geodynamic or paleoclimate forcing, it is necessary to perform absolute dating of appropriate mineral components of ferruginous duricrusts, such as goethite and hematite (Théveniaut and Freyssinet, 1999; Théveniaut and Freyssinet, 2002; Shuster et al., 2005; Monteiro et al., 2014; Allard et al., 2018; Vasconcelos et al., 2019). Through (U-Th)/He geochronology, the knowledge on their timing of formation is continuously increasing, but the chronology of ancient landscapes worldwide in relation to paleoclimatic events is still fragmented and remains a topical issue (Shuster et al., 2005, Shuster et al., 2012;

45   Vasconcelos et al., 2013; Monteiro et al., 2014; Allard et al. 2018; Monteiro et al., 2018; Heller et al., 2022).

In the (U-Th)/He dating methodology, sample mineralogy is analyzed using conventional X-ray diffraction (XRD) and Scanning Electron Microscopy (SEM) on milli/microfacies first recognized through their color and texture by the naked eye or with a binocular magnifier. However, the finely divided nature of iron oxides and oxyhydroxides implies that even inframillimetric grains used for dating (typically less than 500 µm large) can be polycrystalline. Thus, they may exhibit a

50   mineralogical composition that is different from that of the sample otherwise analyzed beside with conventional XRD or SEM. This may induce some bias when interpreting and discussing the (U-Th)/He results, especially when goethite and hematite exhibit contrasting ages according to the sampled microfacies (Anand and Gilkes, 1987).

Classical mineralogical investigations cannot be performed easily on the same sample as the one used for (U-Th)/He dating: SEM can contaminate the grain by metal coating or fixing, and conventional XRD requires amounts of matter (at least

55   several mg of powder) much higher than that of a single grain extracted for (U-Th)/He dating. Consequently, in order to support interpretation and discussion of (U-Th)/He ages of iron oxides and oxyhydroxides generations from ferruginous duricrusts with mineralogy, it appears critical to analyze the same single grain that will be subsequently used for (U-Th)/He dating. This can be potentially achieved using a powerful source of X-rays that is far beyond classical setups, such as those available from a rotating anode (XRD_rotat) in a laboratory or a synchrotron facility (XRD_synch).

60   Consequently, the present study objectives are twofold. First, we propose to refine the mineralogical characterization of iron oxides and oxyhydroxides from ferruginous duricrusts on inframillimetric (*circa* 500 µm), undisturbed grains prior to dating the same grains by (U-Th)/He method. On two contrasting natural samples from a Brazilian pisolitic duricrust (Alto Paranaíba region, Minas Gerais State), the XRD_rotat patterns are compared to the better-resolved XRD_synch patterns. Related data allowed us to determine parameters that are useful to recognize distinct generations of iron phases (i.e., Mean

65 Coherent Domain (MCD) sizes and Al-substitution rate) and the weight percentage (wt%) ratio of the main phases using Rietveld refinement analysis (Bish and Post, 1993). Second, using this methodology, the (U-Th)/He ages of the cortex and core of the pisolitic samples were determined and discussed as an example. Pisoliths are frequently observed in lateritic ferruginous duricrusts, may exhibit contrasting mineralogy between the core and cortex, and are thus relevant for the two objectives of this study. This methodology is shown to be appropriate to evidence and quantify different Fe oxides and

70 oxyhydroxides in dated grains and also potentially to reveal mineral contaminants, provided that their concentration is high enough.

## 2 Material and methods

### 2.1 Sampling site

A lateritic ferruginous duricrusts profile (~1,100 m elevation) developed on relict low-relief uplands in the tropical Brazilian

75 continental interior, Alto Paranaíba region (Minas Gerais State, Brazil), was chosen for sampling. It is developed at the expense of pyroclastic and epiclastic rocks from the Mata da Corda Group (upper Cretaceous) (CPRM, 2014). Despite being an important tropical Brazilian area of occurrence of thick lateritic profiles including duricrusts (Marques et al., 2021), no weathering geochronological data are available yet. The climate of the study area is Aw (Köppen–Geiger's classification), characterized by warm and dry winters, and moist and warm summers. The average annual rainfall is 1,600 mm and the

80 mean annual temperature is 22 °C (Oliveira et al., 2020).

The morphological description of the profile was carried out based on McFarlane (1976), Tardy (1993) and Aleva (1994), and then non-disturbed samples were taken from all the described layers. Based on the morphological description at the fieldwork and laboratory, the pisolitic facies, which is often encountered in lateritic ferruginous duricrusts (Nahon, 1991; Tardy, 1993), was chosen due to being structurally suitable for dating, and also because it presented a usual complexity or

85 heterogeneity allowing us to carry out our methodological approach.

### 2.2 Selection and preparation of samples

The morphological characteristics of a hand specimen from the pisolitic facies were observed and described using a binocular microscope. The populations of iron oxides were identified based on texture, color and morphology (Tardy, 1993), and then the pisoliths were individualized. The semi-quantitative composition of a complete pisolite was analyzed by a Zeiss

90 Ultra55 SEM with a FEG-Schottky electronic source coupled with an energy-dispersive spectrometer (EDS) facility. The working distance was at 7.5 mm and the acceleration voltage was at 15 kV.

Another pisolite with similar morphological characteristics and belonging to the same identified population was sampled using a diamond micro drill to divide the cortex and core. Grains (*circa* 500 µm large) were carefully selected from the cortex and core using an optical microscope. Some of the grains were prepared by hand grinding using a mortar and pestle

95 and then homogenized, and sieved at 100 µm in order to obtain powder samples (~0.50 mg). In the other selected grains (~0.10 mg), no preparation was carried out.

## 2.3 X-ray diffraction data collection and analysis

Both powder samples and single polycrystalline grain samples from the pisolitic cortex and core were analyzed for their mineralogical composition using XRD. Samples were loaded in borosilicate capillaries either as powder fillings or as stuck-
100 up grains. Laboratory X-ray experiments were performed at the X-ray diffraction platform of the *Institut de Minéralogie, de Physique des Matériaux et Cosmochimie* (IMPMC), Sorbonne Université (Paris, France). The single polycrystalline grain samples from the pisolitic core were first analyzed using a Panalytical XpertPro MPD 2-circle diffractometer (Co sealed tube in Debye-Scherrer transmission geometry - $\lambda K\alpha1$= 1,789010 Å, $\lambda K\alpha2$= 1,792900 Å - at 45 KeV and 40 mA, with a range scan of 3-90 °2θ and a step size of 0.03 °2θ s$^{-1}$). The signal collected from the grain was too low, even after several hours of
105 exposure (Fig. S2). Therefore, more intense and collimated sources were required to analyze small grains in transmission geometry.

A Rigaku MM007HF diffractometer equipped with Varimax focusing optics, a RAXIS4++ image plate detector placed at a distance of 200 mm from the sample and a Mo rotating anode ($\lambda K\alpha1$= 0.709319 Å and $\lambda K\alpha2$= 0.713609 Å) at 50 KeV and 24 mA was used, with a range scan of 3 to 45 °2θ and the acquisition time of 60 minutes. The Fit2D program (Hammersley,
110 2016) was used for the integration of 2D images into 1D patterns after a calibration with LaB6 standard. Rotating anode generators are one of the most powerful X-ray sources available in the laboratory. In these experimental setting operating under a high vacuum, a cooled rotating surface is continuously irradiated by an intense electron beam (Fig. 1), resulting in an improved signal-to-noise ratio and in the possibility to analyze small samples.
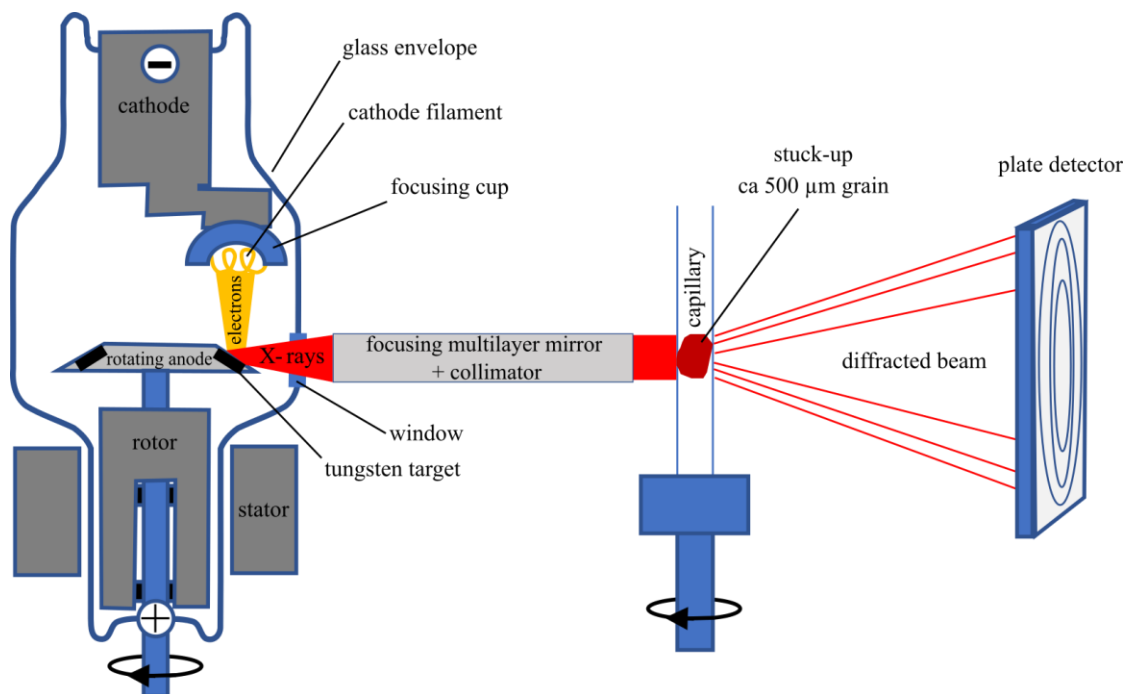
115 **Figure 1: Diagram (out of scale) of the rotating anode X-ray diffraction device.** Samples are loaded in a borosilicate capillary and rotated during the X-ray data collection by an image plate detector at a distance of 200 mm from the sample. A microfocused beam is provided by the multilayer mirror (78 µm) and the inhouse-made collimator.

Higher X-ray fluxes require the use of a synchrotron facility. Therefore, XRD_synch patterns were collected on the same

120 grains at the CRISTAL beamline of the SOLEIL Synchrotron facility (Saint Aubin, France). We used the 2-circle diffractometer of the CRISTAL beamline equipped with a MYTHEN2 X 9K detector (DECTRIS). The measurements were performed in continuous mode at 17 keV (0.72896 or 0.727913 Å) using 5 min exposure time, with a scan range of 3-65 °2θ and a scan speed of 0.04 °2θ s$^{-1}$.

Rietveld refinements of the multiphase XRD patterns were performed with the FullProf software (Rodriguez-Carvajal, 1993)

125 and included hematite, goethite, kaolinite and anatase as mineral phases. Starting crystal structure data were taken from respectively Finger and Hazen (1980), Gualtieri and Venturelli (1999), Bish and Von Dreele (1989) and Howard et al. (1991). Scale factors, cell parameters, isotropic pseudo-Voigt line-profile functions (Thompson-Cox-Hastings) and overall B factors were first refined for the four phases. The peak widths were significantly larger than the instrument resolution (~0.1° 2θ). The instrumental resolution function (IRF) was determined over the 2theta range measured from the LaB6

130 crystallographic standard Rietveld refinement. Assuming that the lorentzian part of the peak broadening is preferentially due to size effect and the Gaussian part to the microstrain, lorentzian isotropic size (Y) and gaussian isotropic strain (U) parameters were refined taking into account the IRF. Then, to improve the fits, anisotropic refinements of size parameters were carried out for hematite, goethite and kaolinite. Regarding hematite, the anisotropic peak broadening has been modeled

as a linear combination of spherical harmonics and every coefficient was refined. This is used to calculate the average
135    apparent sizes in the reciprocal lattice directions corresponding to every fitted Bragg reflection, by applying the Scherrer's
formula (Klug and Alexander, 1974). In order to reduce the number of parameters to refine, we used a needle shape model
elongated along $b$ axis for the goethite and a simplified model of platelet shape perpendicular to $c$ axis for the kaolinite.
Regarding needle-like coherent domain, the obtained value is LorSiz=SZ×sin(phi), where SZ is the refined parameter and
phi is the acute angle between the scattering vector (h,k,l) and the vector defining the needle shape of domains. For platelet
140    coherent domains, LorSiz is assumed to be of the form LorSiz=SZ×cos(phi), where SZ is the refined parameter and phi is the
acute angle between the scattering vector (h,k,l) and the vector defining the platelet shape of domains.

The wt% ratio of the main phases was determined from Rietveld analysis of XRD_rotat and XRD_synch patterns of the
grains, following to classical quantitative mineralogy procedures assuming a sum of mineral weight fractions equal to 1
(Snyder and Bish, 1989). When possible, $Al^{3+}$ for $Fe^{3+}$ substitution rate in goethite and hematite of grain samples were
145    determined by applying the empirical formula by Schulze (1984) and Schwertmann et al. (1979) using $c$ and $a$ unit-cell
parameter values for goethite and hematite, respectively. Occupancy factors for Al and Fe were also refined to improve the
fit quality, but not used for estimating Al-substitution rate since occupancy factors can be significantly affected by non-
stoichiometry in soil iron-oxyhydroxides that typically form at low temperature (Stanjek and Schwertmann 1992; Wolska
and Schwertmann 1993). Therefore, we have been able to compare XRD_rotat and XRD_synch data and evaluate the
150    possibility of mineralogically characterizing grains prior to dating.

The undisturbed grains from the pisolitic core and cortex were undergone to different exposure times (30, 60, 90 min) during
XRD_rotat recording, to find the best conditions for X-ray analysis and verify that (U-Th)/He dating was not biased by He
diffusion.

## 2.4 (U-Th)/He geochronology analysis

155    The grains previously analyzed at different acquisition times by XRD_rotat were weighed, their size was measured, and they
were encapsulated into a niobium tube. Four grains from each population without exposure to irradiation were also analyzed
in order to verify the reliability of our results. Grains with *circa* 500 µm size were selected to avoid significant natural He
losses by alpha ejection (Farley et al., 1996). The aliquots were dated by the (U-Th)/He method at the GEOPS, Paris-Saclay
University, France, following the protocols described in Allard et al. (2018) and Gautheron et al. (2021). The Nb tubes were
160    heated at low temperature <1,000 °C using a diode laser in order to avoid any possible U loss by volatilization (Vasconcelos
et al., 2013) and the $^4$He content of the encapsulated grains was analyzed using a Pfeiffer Prisma Quadrupole mass
spectrometer. More details can be founded in Gautheron et al. (2021). Afterward, grains inside Nb tubes were dissolved by
adding 50 µL of 5N $HNO_3$ containing $^{235}$U, $^{230}$Th and $^{149}$Sm, 50 µL of 5N $HNO_3$, 400 µL of 40 % concentrated HCl, and 100
µL of 38 % HF into 5 mL PFA capped vials (Savillex). The tightly closed vials were heated at about 100 °C overnight. The
165    opened-cap vials were then placed on a hot plate at 100 °C during two hours for complete evaporation. A 1.9 mL volume of
1N $HNO_3$ was added to the solution. The solution was heated at 100 °C to reflux for two hours. After cooling, 1.5 mL of the

6

solution was taken and diluted with 1N $HNO_3$ to reach a total volume of 3 mL. Finally, $^{238}U$, $^{232}Th$, and $^{147}Sm$ content were obtained by using a high-resolution inductively coupled plasma mass spectrometer HR-ICP-MS (ELEMENT XR - Thermofisher Scientific). An analytical error of 5% at $1\sigma$ is expected for the two-steps analysis based on Durango apatite

170    dating uncertainties associated with the analysis made in parallel to the goethite. A 10% correction related to He loss, which is associated with the polycrystalline nature of goethite and hematite samples has been applied, with an error of 10%.

## 3 Results and discussion

### 3.1 Morphological description

The ferruginous duricrust profile of the studied site (see Fig. 2a for location) comprises a ferruginous duricrust *stricto sensu*

175    (~400 cm) transitioning upwards to a pisolite-rich (~100 cm) and nodular indurated zone (~30 cm) (Fig. 2b). The pisoliths are well-formed, irregular in size and shape, and range from 5 to 10 mm in diameter (Fig. 2c). They are linked together by a matrix composed of goethite, kaolinite and quartz. The pisoliths present a concentric yellow-brown cortex that develops at the boundary of the purple-red core with a ferruginized zone (i.e., transition zone) between them. The well-developed concentric cortex presents an alternation of light and dark banded zones (Fig. 2d), where the light rings register a higher Al

180    and Si than Fe content (Fig. 2e), as often observed for pisoliths from duricrusts (Nahon, 1976; McFarlane, 1983; Amouric et al., 1986; Anand and Gilkes, 1987).
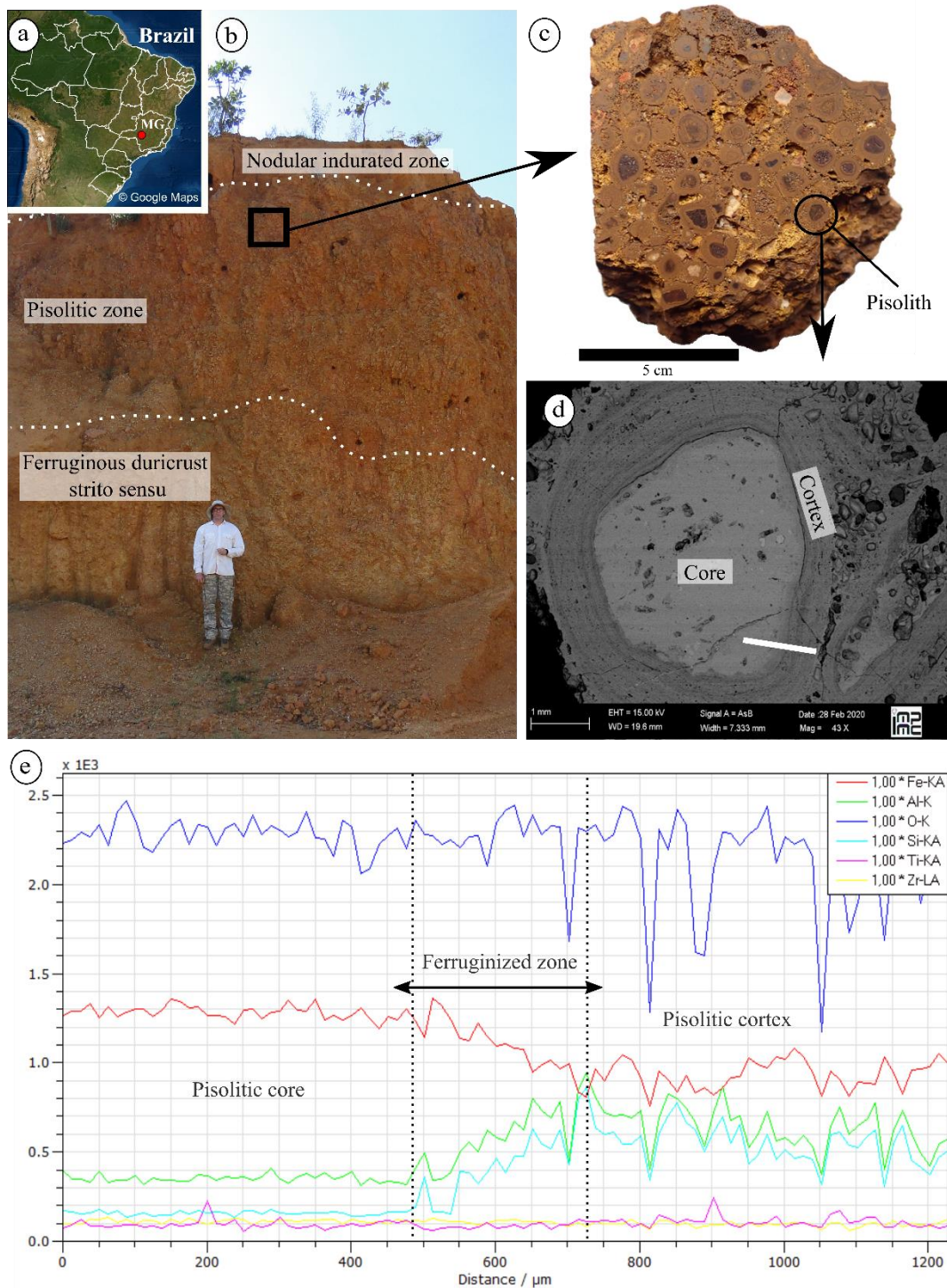
**Figure 2: Ferruginous duricrusts profile and pisolitic facies.** (a) Location of the Fe-duricrust profile in a Brazilian landscape, (b) distinct horizons of the profile, (c) pisolitic facies, (d) internal structure of a pisolith and (e) contrasting compositional variation from the core to cortex. Line white on the SEM image in panel d indicates the transect analyzed and shown in panel e.

## 3.2 XRD analysis of the core and cortex from the pisolitic facies

### 3.2.1 Rotating anode-XRD patterns

Various assays of the XRD_rotat acquisition of grain samples from both pisolitic core and cortex were carried out using 30,
190   60, and 90 min exposure times in order to evaluate the quality of signal/noise in XRD patterns and to question the influence
on He loss by diffusion and (U-Th)/He age. The XRD_rotat patterns of all samples were similar with a significantly high
signal-to-noise ratio (Fig. S1). In addition, the excellent quality of the XRD_rotat patterns is clearly evidenced by comparing
standard XRD on capillaries for the grain and the powder samples (Fig. S2). In particular, a 15 h collection pattern on a grain
does not exhibit significant diffraction peaks. A 60 min exposure time was chosen for XRD_rotat as it provided good quality
195   patterns for Rietveld refinement analysis.

The XRD_rotat patterns for grain and powder samples from the pisolitic core and cortex are shown in Fig. 3, with assigned
mineral contributions. The grain- and powder-XRD patterns were predominantly similar, indicating that both types of
sample preparation could be used to analyze the mineralogical composition for small sample amounts (Fig. 3). However, the
intensity of some peaks appears different for powder and grain samples, suggesting that their mineralogical content may not
200   fully match. Indeed, the core sample shows a relative intensity of hematite (Hm) peaks slightly greater in the grain pattern
than in the powder preparation (Fig. 3). This indicates a heterogeneous Hm content in the selected core microfacies and
strongly justifies the benefit of analyzing the mineralogy of an individual grain before (U-Th)/He geochronological analysis.
Finally, we attest that XRD_rotat provides quality patterns on isolated *circa* 500 µm grains without perturbation. In these
conditions, the grain can then be exposed to a next-step analysis with no risk of data bias.
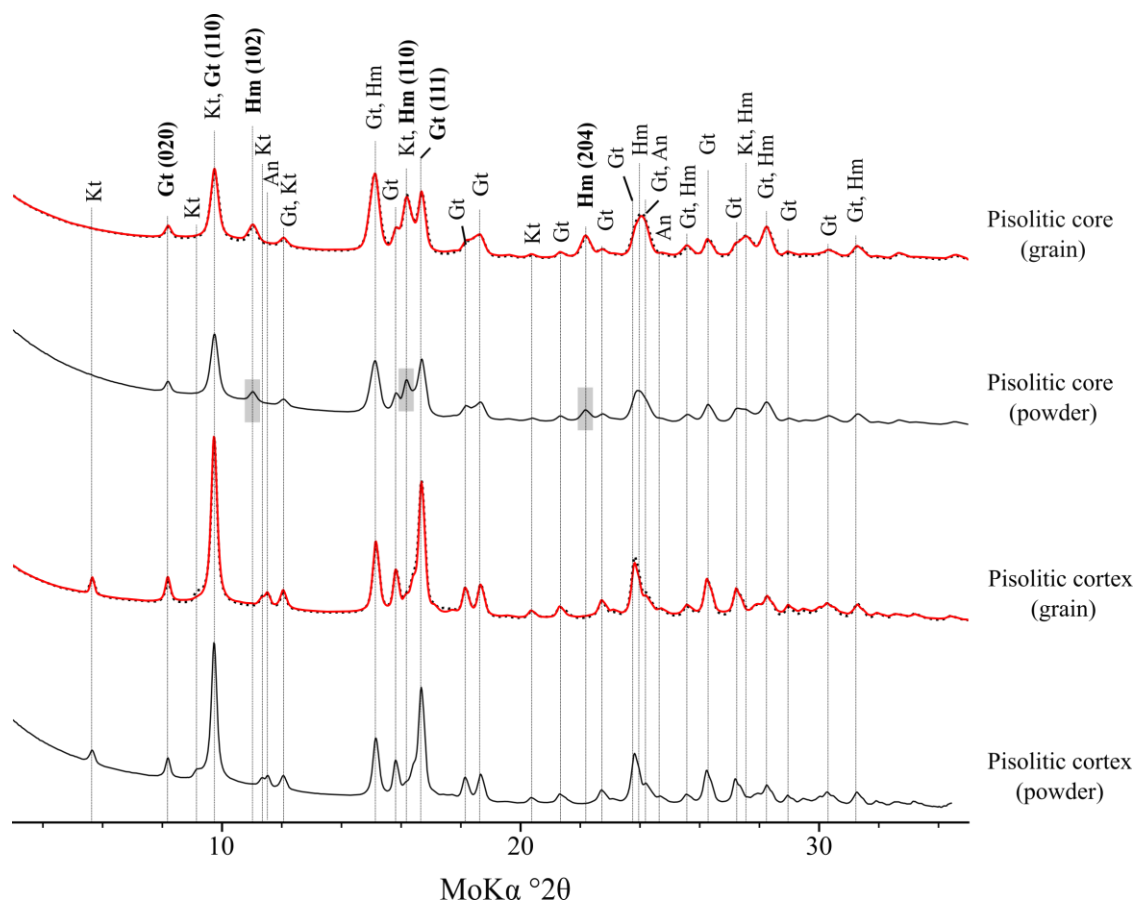
**Figure 3: Rotating anode XRD patterns for grain and powder samples from the pisolitic core and cortex of the ferruginous duricrust.** Gt: goethite, Hm: hematite, Kt: kaolinite and An: anatase. Note that the quality of the grain pattern is similar to that of the powder pattern. The red line represents the Rietveld fit. Grey areas correspond to isolated Hm peaks that vary between grain and powder patterns.

The XRD_rotat patterns indicate that hematite and goethite are present in the pisolitic core whereas goethite and kaolinite are present in the cortex. Kaolinite is revealed by the peaks at 5.69 and 11.37 °2θ (Dixon and Weeds, 1989), which are not observed in the pisolitic core pattern (Fig. 3). The absence of kaolinite in the pisolitic core is often related to its epigenetic replacement by hematite, which becomes more aluminous with the progressive dissolution of kaolinite (Nahon, 1976; Didier, 1983; Didier et al., 1983; Tardy and Nahon, 1985; Ambrosi et al., 1986). The reflection peak at 22.2 °2θ related to (204) hematite was not observed in the XRD_rotat patterns of the pisolitic cortex, regardless of the sample preparation method, indicating a low amount or absence of hematite, as confirmed by the Rietveld refinement (Table 1). The mineralogical composition of the pisolitic core and cortex is consistent with previous studies (Didier et al., 1985; Amouric et al., 1986; Tardy, 1993).

220 **Table 1: Mineralogical parameters determined for the core and cortex samples by Rietveld refinement of XRD_rotat and XRD_synch patterns:** wt% ratio of the main phases, Mean Coherent Domains sizes of the hematite and goethite and $Al^{3+}$ for $Fe^{3+}$ substitution rate in goethite and hematite

| Sample | Hm | Gt | Kt | An | MCD[1] | | Al[2] | |
|---|---|---|---|---|---|---|---|---|
| | | | | | Gt | Hm | Gt | Hm |
| | %wt | | | | nm | | %mol | |
| | | | | XRD_rotat | | | | |
| Core grain | 41 (3.8) | 59 (4.9) | 0.0 | 0.0 | 15 | 12 | 9 | 1 |
| Cortex grain | 0.3 (0.2) | 95 (3.5) | 2.7 (0.3) | 2.5 (0.4) | 23 | * | 4 | * |
| | | | | XRD_synch | | | | |
| Core grain | 32 (0.4) | 68 (1.) | 0.0 | nd | 16 | 18 | 12 | 7 |
| Cortex grain | 0.7 (0.1) | 94 (1.0) | 5.3 (0.3) | nd | 30 | * | 11 | * |

[1] Mean Coherent Domain sizes according to Scherrer's formula; [2] Isomorphic substitution of $Fe^{3+}$ by $Al^{3+}$ according to Schulze (1984) for goethite and Schwertmann et al. (1979) for hematite. Hm: hematite; Gt: goethite; Kt: kaolinite; An: anatase; nd: not determined; * absent.

225

In the grains, the wt% ratio of the main phases indicates that the pisolitic core contains 41% of hematite while the pisolitic cortex is predominantly goethite (i.e., 95%) (Table 1). The Mean Coherent Domain (MCD) size from XRD_rotat is *circa* 15 nm for core goethite and *circa* 12 nm for the core hematite, and *circa* 23 nm for the cortex goethite (Table 1). The MCD sizes for goethite and hematite crystals are in agreement with those reported for other studies, with ranges within 10-40 nm

230 for goethite and from 4-10 nm for hematite (e.g., Tardy and Nahon, 1985; Amouric et al., 1986; Anand and Gilkes, 1987). $Al^{3+}$ for $Fe^{3+}$ substitution rate is 9% in core goethite, 1% in core hematite, and 4% in cortex goethite (Table 1), suggesting a decrease of $Al^{3+}$ for $Fe^{3+}$ substitution rate in goethite from the pisolitic core to cortex.

### 3.2.2 Synchrotron-XRD patterns

The synchrotron X-Ray Diffraction (XRD_synch) patterns for the grain samples from the pisolitic core and cortex were

235 similar to those obtained by XRD_rotat data concerning the signal/noise ratio and identified mineral phases (Fig. 4). As expected, the synchrotron XRD patterns show a better resolution of diffraction peaks than XRD_rotat (Figs. 3 and 4). This can be related to the monochromatic wavelength of the incident synchrotron radiation and higher brilliance, which is useful for identifying minor constituents in a sample and particles of small size (Lombi and Susini, 2009; Tso et al., 2013). Rietveld refinement provided a good fit for all the peaks, except for those corresponding to kaolinite because stacking disorder is not

240 accounted for the code (Fig. 4).
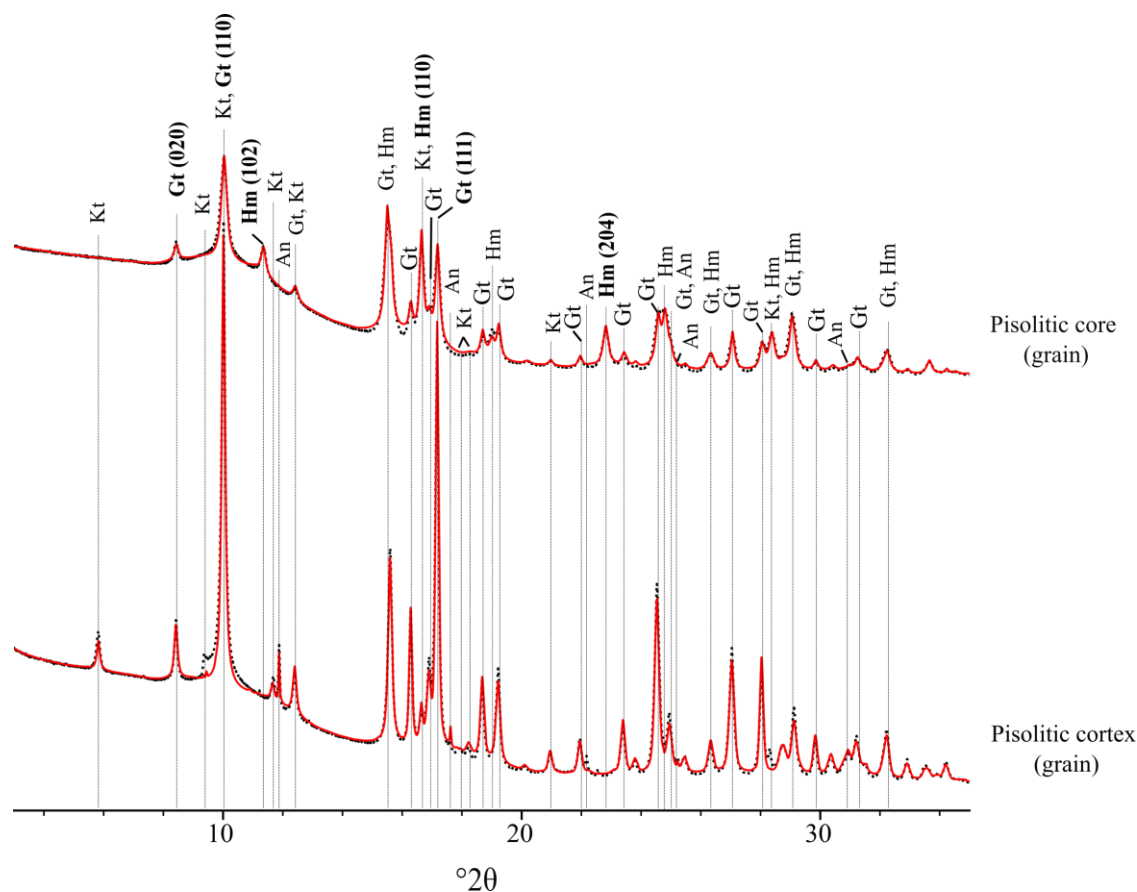
**Figure 4: Synchrotron XRD patterns for grain samples from the pisolitic core and cortex.** Gt: goethite, Hm: hematite, Kt: kaolinite, and An: anatase. The red line represents the Rietveld fit.

245 The wt% ratio of the main phases from XRD_synch data for core grain is consistent with that determined on XRD_rotat pattern (Table 1): a difference of 9% is observed in the core grain and $\leq$ 1% for the cortex grain. In addition, the MCD sizes were quite similar by both XRD data (Table 1). $Al^{3+}$ for $Fe^{3+}$ substitution rate in goethite for core and cortex sample was 12% and 11%, respectively. For the hematite core it was 7%. These values are higher than those observed from XRD_rotat (Table 1).

250 Despite the different settings between XRD_rotat and XRD_synch, both methods are suitable for investigating the mineralogical composition of supergene phases in small amounts (*circa* 500 µm size). The XRD_rotat, available in laboratories, is powerful enough to analyze undisturbed grains that can be subsequently used for dating, and thus appears much more appropriate than conventional XRD analysis that fails analyzing single grains.

12

### 3.2.3 (U-Th)/He analysis

255    The effect of exposure time of XRD_rotat recording on apparent age for pisolitic core and cortex is shown in Fig. 5, and (U-Th)/He data are reported in Table 2. For each sample, there is no representative shift in age related to the acquisition time of mineralogical data: the results show a good reproducibility within the analytical uncertainty, i.e., 5%. Figure 5 clearly shows that all the samples exhibit apparent age clusters including the 0 exposure point, supporting the idea that performing XRD_rotat mineralogical analysis prior (U-Th)/He geochronological analysis is possible without impacting He diffusion and

260    age.
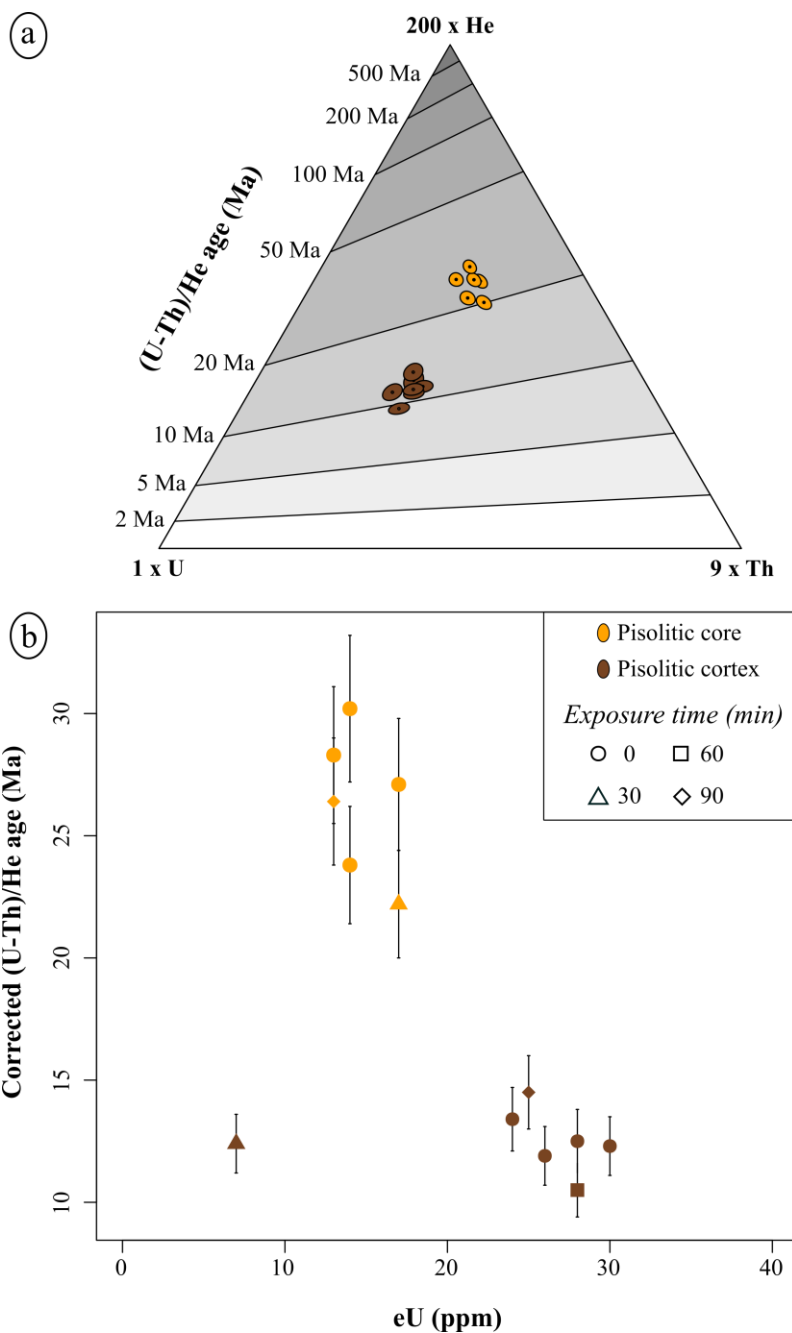
**Figure 5: (U-Th)/He data.** (a) Ternary diagram indicating the He-Th-U concentrations and the (U-Th)/He ages (Ma) for pisolitic core and cortex obtained in the R environment using the "*Helioplot*" function (Vermeesch, 2010); and (b) evolution of the (U-Th)/He age as a function of the effective uranium content (eU=U+0.238×Th + 0.0012×Sm: Cooperdock et al., 2019).

| Sample | Exposure time | Weight | ⁴He | s | ²³⁸U | ²³²Th | ¹⁴⁷Sm | ⁴He | s | ²³⁸U | ²³²Th | ¹⁴⁷Sm | eU | Th/U | Raw age | ± s | Corrected age |
|---|---|---|---|---|---|---|---|---|---|---|---|---|---|---|---|---|---|
| | min | µg | mol | mol | ng | ng | ng | nmol/g | nmol/g | ppm | ppm | ppm | ppm | | Ma | Ma | Ma |
| Durango | 0 | 29 | 6.7E-13 | 1.3E-14 | 0.69 | 14.12 | 1.27 | 22.69 | 0.05 | 23.4 | 480.2 | 43.2 | 139 | 20.6 | 30.7 | 1.6 | 33.8 |
| Durango | 0 | 13 | 2.2E-13 | 4.4E-15 | 0.22 | 4.99 | 0.52 | 16.64 | 0.05 | 16.7 | 375.1 | 38.8 | 107 | 22.5 | 29.3 | 1.6 | 32.2 |
| Durango | 0 | 29 | 5.3E-13 | 1.1E-14 | 0.53 | 11.44 | 1.12 | 17.98 | 0.02 | 17.9 | 388.0 | 38.1 | 111 | 21.6 | 30.4 | 1.6 | 33.4 |
| Durango | 0 | 46 | 1.0E-12 | 2.1E-14 | 1.04 | 22.56 | 1.75 | 22.65 | 0.02 | 22.7 | 494.7 | 38.5 | 142 | 21.8 | 30.1 | 1.5 | 33.1 |
| Durango | 0 | 64 | 1.9E-12 | 3.8E-14 | 2.03 | 39.66 | 3.82 | 29.68 | 0.05 | 31.6 | 618.0 | 59.5 | 180 | 19.6 | 31.0 | 1.6 | 34.1 |
| Durango | 0 | 55 | 1.2E-12 | 2.3E-14 | 1.21 | 23.90 | 2.77 | 21.15 | 0.03 | 22.0 | 433.9 | 50.3 | 126 | 19.7 | 31.5 | 1.6 | 34.6 |
| Core | 0 | 81 | 1.3E-13 | 2.6E-15 | 0.31 | 3.43 | 0.04 | 1.61 | 0.00 | 3.8 | 42.3 | 0.5 | 14 | 11.2 | 21.6 | 0.7 | 23.8 |
| Core | 0 | 147 | 2.7E-13 | 5.4E-15 | 0.59 | 5.69 | 0.09 | 1.83 | 0.00 | 4.0 | 38.7 | 0.6 | 13 | 9.6 | 25.7 | 0.8 | 28.3 |
| Core | 0 | 148 | 3.3E-13 | 6.6E-15 | 0.62 | 7.80 | 0.21 | 2.21 | 0.00 | 4.2 | 52.7 | 1.4 | 17 | 12.5 | 24.6 | 0.8 | 27.1 |
| Core | 0 | 149 | 3.1E-13 | 6.1E-15 | 0.54 | 6.44 | 0.12 | 2.05 | 0.00 | 3.6 | 43.2 | 0.8 | 14 | 12.0 | 27.5 | 0.9 | 30.3 |
| Core | 30 | 279 | 5.0E-13 | 1.0E-14 | 1.08 | 14.98 | 0.13 | 1.80 | 0.00 | 3.9 | 53.7 | 0.5 | 17 | 13.9 | 20.2 | 0.6 | 22.2 |
| Core | 90 | 114 | 2.0E-13 | 3.9E-15 | 0.36 | 4.89 | 0.05 | 1.71 | 0.00 | 3.1 | 42.9 | 0.4 | 13 | 13.8 | 24.0 | 0.8 | 26.4 |
| Cortex | 0 | 177 | 2.7E-13 | 5.4E-15 | 1.72 | 10.31 | 0.29 | 1.55 | 0.05 | 9.7 | 58.3 | 1.7 | 24 | 6.0 | 12.2 | 1.5 | 13.4 |
| Cortex | 0 | 138 | 2.3E-13 | 4.6E-15 | 1.47 | 9.79 | 0.42 | 1.68 | 0.01 | 10.7 | 70.9 | 3.1 | 28 | 6.6 | 11.4 | 0.4 | 12.5 |
| Cortex | 0 | 136 | 2.0E-13 | 4.0E-15 | 1.41 | 8.60 | 0.28 | 1.48 | 0.00 | 10.4 | 63.2 | 2.1 | 26 | 6.1 | 10.8 | 0.3 | 11.9 |
| Cortex | 0 | 145 | 2.6E-13 | 5.2E-15 | 1.76 | 10.64 | 0.33 | 1.79 | 0.00 | 12.2 | 73.4 | 2.3 | 30 | 6.0 | 11.2 | 0.4 | 12.3 |
| Cortex | 30 | 36 | 1.6E-14 | 3.1E-16 | 0.12 | 0.58 | 0.02 | 0.44 | 0.00 | 3.3 | 16.2 | 0.6 | 7 | 4.9 | 11.3 | 0.5 | 12.4 |
| Cortex | 60 | 48 | 6.8E-14 | 1.4E-15 | 0.58 | 3.12 | 0.08 | 1.42 | 0.01 | 12.2 | 64.9 | 1.8 | 28 | 5.3 | 9.5 | 0.3 | 10.5 |
| Cortex | 90 | 197 | 3.4E-14 | 6.8E-16 | 2.05 | 12.10 | 0.34 | 1.77 | 0.04 | 10.4 | 61.4 | 1.7 | 25 | 5.9 | 13.2 | .6 | 14.5 |

265 **Table 2: Raw and corrected (U-Th)/He age for the investigated iron-oxides and oxyhydroxides and Durango standard apatite**

270　U and Th concentrations clearly differ between the pisolitic core and cortex, with higher values of both elements occurring in the pisolitic cortex. This suggests a relative U enrichment during the weathering of the iron oxides and oxyhydroxides from the core (Fig. 5). A grain from the pisolitic cortex (with 30 min exposure) contains lower U and Th concentrations than other grains (Fig. 5b), which can be explained by small differences between grains, as it generally occurs for grains of supergene minerals belonging to the same population (e.g., Vasconcelos et al., 2013; Monteiro et al., 2014; Riffel et al., 2016; Heller et al., 2022). Nevertheless, such difference does not influence the age, when compared to the other grains of the same

275　micro/millifacies (Fig. 5b).

Corrected (U-Th)/He ages for the pisolitic core range from 30±3.0 to 22±2.2 Ma and pisolitic cortex from 15±1.5 to 11±1.1 Ma (Table 2). The apparent age reveals that the pisolitic core is older than the pisolitic cortex, being this fully in agreement with the model that takes into account the development of pisoliths coming from different localities and proposed by several authors (e.g., Didier et al., 1983; Didier et al., 1985; Tardy and Nahon, 1985; Nahon and Tardy, 1992). It must be pointed out

280　that the core age may be considered as an average age of the hematite and goethite, with hematite being possibly hypothetically older than goethite. MCD sizes and $Al^{3+}$ for $Fe^{3+}$ substitution rate in goethite from the core and cortex rather indicate that they formed in different conditions (Table 1), but with no constraint on the age. According to the (U-Th)/He age of the pisolitic core, a first formation episode of ferruginous duricrusts at the Alto Paranaíba region (Minas Gerais State, Brazil) occurred at, or before, the Oligocene, which indicates a period of optimal climate conditions in the study area, as

285　already reported in a surrounding area (Monteiro et al., 2014; 2018), even though more data are needed to relate the paleoclimates and mineral precipitation. Our results suggest, in addition, that a secondary weathering formation process took place from the middle Miocene (~15 to 11 Ma) (Table 1). Other studies also identified distinct weathering episodes in Brazilian territory (e.g., Monteiro et al., 2014; Riffel et al., 2016; Allard et al., 2018; Monteiro et al.,2018; Vasconcelos et al., 2019). However, additional data are needed to further discuss the evolution of the studied duricrust.

290　**3 Conclusions**

Mineralogy of supergene phases from core and cortex of a pisolitic facies can be explored on submillimetric (≤500 μm) single grains by XRD_rotat, which is a non-destructive method, yielding high quality patterns, while standard XRD is not relevant. Rietveld refinement outputs such as phase concentrations or Mean Coherent Domain sizes showed results consistent with XRD_synch. The grains analyzed by XRD_rotat do not exhibit X-ray exposure effects and they are then

295　suitable for further-step analysis such as (U-Th)/He dating. This approach could potentially be applied to other mineral parageneses (e.g., Mn-oxides, jarosites) prior to dating.

Although investigated over a small series of grains, corrected (U-Th)/He ages of pisolitic core ranging from ~30 to 22 Ma revealed that a first formation episode of ferruginous duricrusts at the Alto Paranaíba region (Minas Gerais State, Brazil) occurred at or before the Oligocene. A subsequent phase associated with a secondary weathering formation process took

300　place from the middle Miocene, which is highlighted by the formation of the goethitic pisolitic cortex. Therefore, the

apparent age by (U-Th)/He results reveals that the pisolitic core is older than the pisolitic cortex, agreeing with the model previously proposed on the development of pisoliths in duricrusts.

**Data availability**

All data generated or analysed during this study are included in this manuscript or its supplementary material.

305  **Author contribution**

Karina P. P. Marques, Thierry Allard, Cécile Gautheron and Guillaume Morin conceptualized the research and designed the methodology. Karina P. P. Marques carried out laboratory analysis and data interpretation. Benoît Baptiste supported laboratory analysis including Rietveld refinement. Ludovic Delbes and Rosella Pinna-Jamme participated to mineralogical and (U-Th)/He analysis, respectively. Pablo Vidal-Torrado made acquisition of the financial support for the project. Karina

310  P. P. Marques, Thierry Allard and Cécile Gautheron wrote the manuscript and integrated contributions from all co-authors.

**Competing interests**

The third author is a member of the editorial board of Geochronology. The other authors have no competing interests to declare.

# References

Aleva, G.J.J. (Ed.): Laterites: Concepts, Geology, Morphology and Chemistry, International Soil Reference and Information Centre, Wageningen (Netherlands), 1994.

330 Allard, T., Gautheron, C., Riffel, S.B., Balan, E., Soares, B.F., Pinna-Jamme, R., Derycke, A., Morin G., Bueno, G.T. and Nascimento, N.: Combined dating of goethites and kaolinites from ferruginous duricrusts. Deciphering the Late Neogene erosion history of Central Amazonia, Chemical Geology, 479, 136-150, https://doi.org/10.1016/j.chemgeo.2018.01.004, 2018.

Ambrosi, J.P., Nahon, D. and Herbilon, A.J.: The epigenetic replacement of kaolinite by hematite in laterite. Petrographic 335 evidence and the mechanisms involved, Geoderma, 37, 283-294, https://doi.org/10.1016/0016-7061(86)90030-3, 1986.

Amouric, M., Baronneta., A., Nahon, D. and Didier, P.: Electron microscopic investigations of iron oxyhydroxides and accompanying phases in lateritic iron-crust pisolites, Clays Clay Minerals, 34, 45-52, 1986.

Anand, R.R. and Gilkes, R.J.: Variations in the properties of iron oxides within individual specimens of lateritic duricrust, Aust. J. Soil Res., 25, 287-302, https://doi.org/10.1071/SR9870287, 1987.

340 Beauvais, A. and Chardon, D.: Modes, tempo, and spatial variability of Cenozoic cratonic denudation: The West African example, Geochemistry, Geophysics, Geosystems, 14, 1590-1608, https://doi.org/10.1002/ggge.20093, 2013.

Bish, D.L. and Post, J.E.: Quantitative mineralogical analysis using the Rietveld full-pattern fitting method, Amer. Miner., 78, 932–940, 1993.

Bish, D.L. and Von Dreele, R.B: Rietveld refinement of non-hydrogen atomic positions in kaolinite, Clays and Clay 345 Minerals, 37, 289-296, https://doi.org/10.1346/CCMN.1989.0370401, 1989.

Cooperdock, E.H., Ketcham, R.A. and Stockli, D.F.: Resolving the effects of 2D versus 3D grain measurements on (U-Th)/He age data and reproducibility, Geochronology, 1, 17-41, https://doi.org/10.5194/gchron-1-17-2019, 2019.

CPRM - SERVIÇO GEOLÓGICO DO BRASIL: Mapa geológico do Estado de Minas Gerais - 1:1.000.000, CPRM, Belo Horizonte, 2014.

350 Didier, P.: Paragenèses à oxydes et hydroxydes de fer dans les bauxites et les cuirasses ferrugineuses, Thèse 3e cycle, Univ. Poitiers, France, 150 pp., 1983.

Didier, P., Nahon, D., Fritz, B. and Tardy, Y.: Activity of water as a geochemical controlling factor in ferricretes. A thermodynamic model in the system: kaolinite Fe-Al-oxihydroxides, Sei. Géol. Mérn., 71, 35 – 44, 1983.

Didier, P., Perret, D., Tardy, Y. and Nahon, D.: Equilibres entre kaolinites ferrifères, goethites alumineuses et hématites 355 alumineuses dans les systèmes cuirasses rôle de l'activité de l'eau et de la taille des pores, Sci. Géol. Bull., 38, 383-397, 1985.

Dixon, J.B. and Weeds, S.B. (Eds.): Minerals in Soil Environments, Soil Science Society of America, Madison, WI, 1989.

Farley, K.A., Wolf, R.A. and Silver, L.T.: The effects of long alpha-stopping distances on (U-Th)/He ages, Geochimica et Cosmochimica Acta, 60, 4223-4229, https://doi.org/10.1016/S0016-7037(96)00193-7, 1996.

Finger, L.W. and Hazen, R.M.: Crystal Structure and Isothermal Compression of $Fe_2O_3$, $Cr_2O_3$, and $V_2O_3$ to 50 Kbars,

360     Journal of Applied Physics, 51, 5362-5367, http://dx.doi.org/10.1063/1.327451, 1980.

Gautheron, C., Pinna-Jamme, R., Derycke, A., Ahadi, F., Sanchez, C., Haurine, F., Monvoisin, G., Barbosa, D., Delpech, G., Maltese, J., Sarda, P. and Tassan-Got, L.: Technical note: Analytical protocols and performance for apatite and zircon (U–Th)/He analysis on quadrupole and magnetic sector mass spectrometer systems between 2007 and 2020, Geochronology, 3, 351-370, https://doi.org/10.5194/gchron-3-351-2021, 2021.

365     Gualtieri, A. and Venturelli, P.: In situ study of the goethite-hematite phase transformation by real time synchrotron powder diffraction, American Mineralogist, 84, 895-904, https://doi.org/10.2138/am-1999-5-624, 1999.

Hammersley, A.P.: FIT2D: a multi-purpose data reduction, analysis and visualization program, J. Appl. Cryst., 49, 646-652, https://doi.org/10.1107/S1600576716000455, 2016.

Heller, B.H., Riffel, S.B., Allard, T., Morin, G., Roig, J., Couëffe, R., Aertsgeerts, G., Derycke, A., Ansart, C., Pinna-Jamme

370     and Gautheron, C.: Reading the climate signals hidden in bauxite, Geochimica et Cosmochimica Acta, 323, 40-73, https://doi.org/10.1016/j.gca.2022.02.017, 2022.

Howard, C.J., Sabine, T.M. and Dickson, F.: Structural and thermal parameters for rutile and anatase, Acta Crystallographica Section B, 47, 462-468, https://doi.org/10.1107/S010876819100335X, 1991.

Klug, H.P. and Alexander, L.E. (Eds.): X-ray Diffraction Procedures for Polycrystalline and Amorphous Materials, 2nd Ed,

375     John Wiley & Sons, New York, 1974.

Lombi, E. and Susini, J.: Synchrotron-based techniques for plant and soil science: opportunities, challenges and future perspectives. Plant Soil, 320, 1–35, 2009.

Marques, K.P.P., Santos, M., Peifer, D., Silva, C.L. and Vidal-Torrado, P.: Transient and relict landforms in a lithologically heterogeneous post-orogenic landscape in the intertropical belt (Alto Paranaíba region, Brazil), Geomorphology, 391,

380     107892, https://doi.org/10.1016/j.geomorph.2021.107892, 2021.

McFarlane, M.J.: Laterite and Landscape, Academic Press, London, 1976.

McFarlane, M.J.: Laterites, in: Chemical sediments and geomorphology, edited by: Goudie, A.S. and Pye, K., Academic Press, New York, 7-58, 1983.

Monteiro, H.S., Vasconcelos, P.M.P. and Farley, K.A.: A combined (U-Th)/He and cosmogenic [3]He record of landscape

385     armoring by biogeochemical iron cycling, Journal of Geophysical Research: Earth Surface, 123, 298–323, https://doi.org/10.1002/2017JF004282, 2018.

Monteiro, H.S., Vasconcelos, P.M.P., Farley, K.A., Spier, C.A. and Mello, C.L.: (U-Th)/He geochronology of goethite and the origin and evolution of cangas, Geochimica et Cosmochimica Acta, 131, 267–289, https://doi.org/10.1016/j.gca.2014.01.036, 2014.

390     Nahon, D.: Cuirasses ferrugineuses et encroûtements calcaires au Sénégal occidental et en Mauritanie, Mém. Sci. Géol. Strassbourg, 44, 232 pp., 1976.

Nahon, D.: Evolution of iron crusts in tropical landscapes, in: Rates of Chemical Weathering of Rocks and Minerals, edited by Colman, S.M. and Dethier, D.P., Academic Press, New York, 169-191, 1986.

Nahon, D. and Tardy, Y.: The ferruginous laterites, in: Regolith exploration geochemistry in tropical and subtropical terrains, Handbook of exploration geochemistry, edited by Butt, C.R.M. and Zeegerds, H., Elsevier, Amsterdam, 41-55, 1992.

Nahon, D.B.: Introduction to the Petrology of Soils and Chemical weathering, John Wiley & Sons, New York, 1991.

Oliveira, P.E., Raczka, M., McMichael, C.N.H., Pinaya, J.L.D. and Bush, M.B.: Climate change and biogeographic connectivity across the Brazilian cerrado, Journal of Biogeography, 47, 396-407, https://doi.org/10.1111/jbi.13732, 2020.

Ollier, C.D. and Sheth, H.C.: The High Deccan duricrusts of India and their significance for the "laterite" issue, Journal of Earth System Science, 117, 537–551, https://doi.org/10.1007/s12040-008-0051-9, 2008.

Riffel, S.B., Vasconcelos, P.M., Carmo, I.O. and Farley, K.A.: Goethite (U–Th)/He geochronology and precipitation mechanisms during weathering of basalts, Chemical Geology, 446, 18–32, http://dx.doi.org/10.1016/j.chemgeo.2016.03.033, 2016.

Rodriguez-Carvajal, J.: "FullProf Program", Physica B, 192, 55-69, 1993.

Schulze, D.G.: The influence of aluminium on iron oxides. VIII – unit-cell dimensions of Al-substituted goethites and estimation of Al from them, Clays Clay Miner., 32, 36-44, https://doi.org/10.1346/CCMN.1984.0320105, 1984.

Schwertmann, U., Fitzpatrick, R.W., Taylor, R.M. and Lewis, D.G. The influence of aluminum on iron oxides. Part II. Preparation and properties of Al-substituted hematites, Clays Clay Miner., 27, 105–112, https://doi.org/10.1346/CCMN.1979.0270205, 1979.

Shuster, D.L., Farley, K.A., Vasconcelos, P.M.P., Balco, G., Monteiro, H.S., Waltenberg, K. and Stone, J.O.: Cosmogenic $^3$He in hematite and goethite from Brazilian "canga" duricrust demonstrates the extreme stability of these surfaces, Earth and Planetary Science Letters, 329-330, 41–50, https://doi.org/10.1016/j.epsl.2012.02.017, 2012.

Shuster, D.L., Vasconcelos, P.M.P., Heim, J.A. and Farley, K.A.: Weathering geochronology by (U-Th)/He dating of goethite, Geochimica et Cosmochimica Acta, 69, 659–673, https://doi.org/10.1016/j.gca.2004.07.028, 2005.

Snyder R.L. and Bish D.L.: Quantitative analysis, in: Modern Powder Diffraction, Reviews in Mineralogy, vol. 20, edited by Bish, D.L. and Post, J.E. Mineralogical Society of America, Washington, 101-144, 1989.

Stanjek H. and Schwertmann U.: The influence of aluminium on iron oxides. XVI: Hydroxyl and aluminum substitution in synthetic hematites, Clays and Clay Minerals, 40/3, 347-354, https://doi.org/10.1346/CCMN.1992.0400316, 1992.

Tardy, Y. (Ed): Pétrologie des latérites et des sols tropicaux, Masson, Paris, 1993.

Tardy, Y. and Nahon, D.: Geochemistry of laterites, stability of Al-goethite, Al-hematite and $Fe^{3+}$-kaolinite in bauxites and ferricretes: an approach of the mechanism of concretion formation, Am. J. Sci. 285, 865-903, https://doi.org/10.2475/ajs.285.10.865, 1985.

Tardy, Y. and Roquin, C. (Eds.): Dérive des continents. Paléoclimats et altérations tropicales, Éditions BGM, Orléans, 1998.

Théveniaut, H. and Freyssinet, P.: Paleomagnetism applied to lateritic profiles to assess saprolite and duricrust formation
425   processes: the example of Mont Baduel profile (French Guiana), Palaeogeogr. Palaeoclimatol. Palaeoecol., 148, 209–231,
https://doi.org/10.1016/S0031-0182(98)00183-7, 1999.

Théveniaut, H. and Freyssinet, P.: Timing of lateritization on the Guiana shield: synthesis of paleomagnetic results from
French Guiana and Suriname, Palaeogeogr. Palaeoclimatol. Palaeoecol., 178, 91–117, https://doi.org/10.1016/S0031-
0182(01)00404-7, 2002.

430   Tsao, T., Chen, Y., Sheu, H., Tzou, Y., Chou, Y. and Wang, M.: Separation and identification of soil nanoparticles by
conventional and synchrotron X-ray diffraction, Applied Clay Science, 85, 1–7, https://doi.org/10.1016/j.clay.2013.09.005,
2013.

Vasconcelos, P.M. and Carmo, I.D.O.: Calibrating denudation chronology through $^{40}Ar/^{39}Ar$ weathering geochronology,
Earth-Sci. Rev., 179, 411–435, https://doi.org/10.1016/j.earscirev.2018.01.003, 2018.

435   Vasconcelos, P.M., Farley, K.A., Stone, J., Piacentini, T. and Fifield, L.K: Stranded landscapes in the humid tropics: Earth's
oldest land surfaces, Earth and Planetary Science Letters, 519, 152–164, https://doi.org/10.1016/j.epsl.2019.04.014, 2019.

Vasconcelos, P.M.P., Heim, J.A., Farley, K.A., Monteiro, H. and Waltenberg, K.: $^{40}Ar/^{39}Ar$ and (U–Th)/He – $^{4}He/^{3}He$
geochronology of landscape evolution and channel iron deposit genesis at Lynn Peak, Western Australia, Geochimica et
Cosmochimica Acta, 117, 283–312, https://doi.org/10.1016/j.gca.2013.03.037, 2013.

440   Vermeesch, P.: HelioPlot, and the treatment of overdispersed (U-Th-Sm)/He data, Chem. Geol., 271, 108-111,
https://doi.org/10.1016/j.chemgeo.2010.01.002, 2010.

Wolska, E. and Schwertmann, U.: The mecanism of solid solution formation between goethite and diaspore, Neues Jahrbuch
für Mineralogie Monatshefte, 5, 213-223, 1993.